Heat and Mass Transfer 40 (2004) 325–337
DOI 10.1007/s00231-002-0401-0

Heat transfer and flow induced by both natural convection and vibrations inside an open-end vertical channel

A.-R.A. Khaled, K. Vafai

Abstract The effects of oscillatory motions that may present at a wall during vibrating conditions are studied on flow induced by natural convection and heat transfer inside an open-end vertical channel. The governing equations are non-dimensionalized and reduced to simpler forms. Analytical solutions are obtained for several limiting cases. The reduced governing equations are solved for various values of the controlling parameters. It is found that mean values of average Nusselt numbers are mainly affected by the Grashof number and the amplitude of the horizontal vibrations. Further, amplitudes of Nusselt numbers at the vibrated wall are decreased as the Grashof number increases for horizontal vibrations while they are increased as amplitudes of vibrations increase. It is also found that the squeezing/vibrational Reynolds number, Grashof number and amplitudes of vibrations have a great influence on the trends of stream lines and isotherms especially at low Grashof numbers. Finally, correlations that summarize the effects of the different controlling parameters are determined on the Nusselt numbers and their amplitudes at relatively low frequency of vibrations.

Keywords Open-end vertical channel, Natural convection, Squeezing, Shearing, Vibration

B	height of the vertical channel
c_p	specific heat of the fluid
Gr	Grashof number
H, h, h_o	dimensionless, dimensional and reference thickness of the channel
h_c	convective heat transfer coefficient
k	thermal conductivity of the fluid
Nu_L, Nu_R	local Nusselt number at the left and right walls
Pr	Prandtl number
p	fluid pressure
R_S	squeezing/vibrational Reynolds number
T, T_1, T_2	temperature in fluid, right and left wall temperatures
t	time
U, u	dimensionless and dimensional vertical velocities
V, v	dimensionless and dimensional horizontal velocities
v_o	reference wall speed
X, x	dimensionless and dimensional vertical coordinates
Y, y	dimensionless and dimensional horizontal coordinates
Ω, Ω^*	dimensional and dimensionless vorticity
Ψ, Ψ^*	dimensional and dimensionless stream function
β	dimensionless squeezing motion amplitude
β_o	thermal expansion coefficient
ε	perturbation parameter
γ	dimensionless frequency
η	variable transformation for Y-coordinate
μ	dynamic viscosity of the fluid
θ	dimensionless temperature in flow field
θ_{AVG}	dimensionless average temperature at a given X value
ρ	density of the fluid
τ, τ^*	dimensionless time
υ	kinematic viscosity
ω	reference frequency of the vibration
ξ	variable transformation for the X-coordinate

Received: 13 May 2002
Published online: 18 December 2002

A.-R.A. Khaled
Department of Mechanical Engineering, The Ohio State University, Columbus OSU, Ohio 43210, USA

K. Vafai (✉)
Department of Mechanical Engineering, University of California at Riverside UCR, Riverside, CA 92521, USA
E-mail: kambiz.vafai@ucr.edu

1 Introduction

A significant domain of natural convection flows have relatively small velocity magnitudes and contain almost unnoticeable turbulence levels. Spaces cooled by natural convection flows vary from one application to another. Of special interest is vertical channels that are partially opened from the upper end. These can find importance in electrical and electronic cooling applications (see Daloglu and Ayhan [1]) as they may exist between the different electronic cards.

Laminar heat transfer by natural convections has been studied extensively in the literature for different geometries. An example for works related to natural convection in vertical channels is the work of Writz and Stutzman [2] who performed an experimental study of free convection between vertical plates with symmetric heating. Another work that is considered is the work of Ramanathan and Kumar [3] who performed a theoretical study for Natural Convection between Heated Vertical Plates. Many researchers considered natural convections inside open ended enclosures such as Vafai and Ettefaqh [4] and [5] and Khanafer and Vafai [6].

Natural convection inside vertical channels has received increased attention in the past decade. Conjugate conductive and porous medium effects are considered as in the works of Morrone [7] and Paul et al. [8], respectively. Further, the presence of internal sources, mass species and variable properties effects have been taken into account in various works concerning natural convections inside cavities and vertical channels as in the work of Barozzi and Corticelli [9], Kuan-Tzon [10] and the work of Zamora and Hernandez [11], respectively. In addition, turbulent, thermal radiation and two phase flow effects have been encountered recently in the study of natural convection inside vertical channels as in the works of Bessaih and Kadja [12], Hall et al. [13] and Dalal et al. [14], respectively.

There are only few works that have dealt with laminar heat transfer and flow induced by natural convection inside vibrating geometries. As an example, Fu and Shieh [15] studied the effects of the buoyancy and vertical vibrations at the four walls of a square closed cavity.

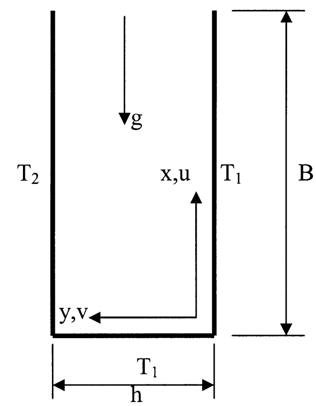

Fig. 1. Schematic Diagram

Further, Kwak [16] discussed the effects of having vibrations on the temperature of one plate of a closed cavity on the natural convection inside the cavity. Although natural convection inside different geometries have been investigated for many effects as shown before, the literature lacks numerical studies that relate the behavior of vertical channels in a vibrated media with both horizontal and vertical vibrations.

In this work, one of the vertical walls is allowed to have oscillatory motions in either the vertical or horizontal directions. These motions model certain modes of vibrations that can occur in vertical channels. This study is performed on an open-end vertical channel. The governing equations such as vorticity-stream function formulations and the energy equation are non-dimensionalized and corresponding dimensionless parameters are introduced. The reduced equations are solved numerically for a wide range of parameters that do not cause any flow instabilities inside the open-end vertical channel. Accordingly, an investigation is done to better understand the performance of natural convection inside vibrated vertical channels.

2
Problem formulation

Consider a two dimensional vertical channel that has a small thickness h compared to its height B. The x-axis is taken in the direction of the height of the vertical channel while y-axis is taken along its thickness as shown in Fig. 1. The bottom of the vertical channel is considered to be closed while the channel is open from the top. The schematic diagram that is shown in Fig. 1 represents the lower portion of a semi-infinite vertical channel chopped at a height equal to B. It is assumed that the flow is laminar and the fluid is Newtonian. Further, the fluid is assumed to have constant properties except for the density which is function of temperature. The right wall of the channel is taken to be fixed while two cases will be considered for the left wall motion as they can model certain modes of vibrations.

Case 1: The motions of the left wall are horizontal motions such that the thickness of the channel is expressed according to:

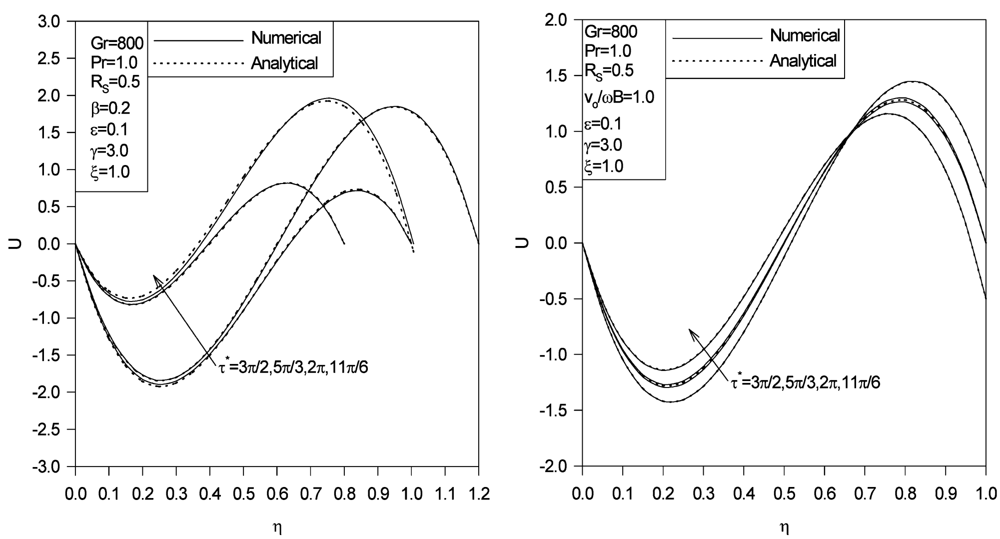

Fig. 2. Validations of Numerical Results: Left wall having oscillatory (a) horizontal and (b) vertical motion

$$h = h_o(1 - \beta \cos(\gamma\omega t)) \tag{1(a)}$$

where h_o, β and ω are the reference channel thickness, left wall motion amplitude and a reference frequency, respectively and γ is the dimensionless frequency.

Case 2: Another case that will be discussed is by considering the motion of the left wall to be in the vertical direction that is a shearing motion. The left wall velocity for this case can be expressed as:

$$u(x, h_o, t) = v_o \sin(\gamma\omega t) \tag{1(b)}$$

where v_o is a reference wall speed.

2.1 General model

The general laminar two-dimensional continuity, momentum and energy equations are given as

$$\frac{\partial u}{\partial x} + \frac{\partial v}{\partial y} = 0 \tag{2}$$

$$\frac{\partial u}{\partial t} + u\frac{\partial u}{\partial x} + v\frac{\partial u}{\partial y} = -\frac{1}{\rho}\frac{\partial p}{\partial x} + \upsilon\left(\frac{\partial^2 u}{\partial x^2} + \frac{\partial^2 u}{\partial y^2}\right) + g\beta_o(T - T_o) \tag{3}$$

$$\frac{\partial v}{\partial t} + u\frac{\partial v}{\partial x} + v\frac{\partial v}{\partial y} = -\frac{1}{\rho}\frac{\partial p}{\partial y} + \upsilon\left(\frac{\partial^2 v}{\partial x^2} + \frac{\partial^2 v}{\partial y^2}\right) \tag{4}$$

$$\rho c_p\left(\frac{\partial T}{\partial t} + u\frac{\partial T}{\partial x} + v\frac{\partial T}{\partial y}\right) = k\left(\frac{\partial^2 T}{\partial x^2} + \frac{\partial^2 T}{\partial y^2}\right) \tag{5}$$

where T, ρ, p, υ, c_p and k are the fluid temperature, density, pressure, kinematic viscosity, specific heat and the thermal conductivity of the fluid, respectively and β_o, T_o and g are the coecient of thermal expansion of the working fluid, reference temperature and the gravitational acceleration. It is worth noting that the Boussinesq approximation is used to approximate the governing momentum equations.

The resulting vorticity-stream function formulations from equations (3) and (4) are

$$\frac{\partial \Omega}{\partial t} + u\frac{\partial \Omega}{\partial x} + v\frac{\partial \Omega}{\partial y} = \upsilon\left(\frac{\partial^2 \Omega}{\partial x^2} + \frac{\partial^2 \Omega}{\partial y^2}\right) - g\beta_o\frac{\partial T}{\partial y} \tag{6}$$

$$\frac{\partial^2 \Psi}{\partial x^2} + \frac{\partial^2 \Psi}{\partial y^2} = -\Omega \tag{7}$$

where Ω and Ψ are the dimensional vorticity and stream functions, respectively. The vorticity and stream functions are related to the velocity components through the following:

$$\Omega = \frac{\partial v}{\partial x} - \frac{\partial u}{\partial y} \tag{8}$$

$$u = \frac{\partial \Psi}{\partial y} \quad v = -\frac{\partial \Psi}{\partial x} \tag{9(a,b)}$$

2.2 Boundary conditions

The dimensional boundary and initial conditions for the first case are

$$\begin{aligned}
&\Psi(0, y, t) = 0, \quad \frac{\partial^2 \Psi(B, y, t)}{\partial x^2} = 0\\
&\Psi(x, 0, t) = 0, \quad \Psi(x, h, t) = -h_o\omega x\beta\gamma \sin(\gamma\omega t)\\
&\Psi(x, y, 0) = 0\\
&u(0, y, t) = 0, \quad u(x, 0, t) = 0, \quad u(x, h, t) = 0\\
&v(0, y, t) = 0, \quad v(x, 0, t) = 0, \quad v(x, h, t) = h_o\omega\gamma\beta \sin(\gamma\omega t)
\end{aligned} \tag{10(a)}$$

$$\begin{aligned}
&\Omega(0, y, t) = -\varepsilon^2\frac{\partial^2 \Psi(0, y, t)}{\partial x^2}, \quad \frac{\partial^2 \Omega(B, y, t)}{\partial x^2} = 0\\
&\Omega(x, 0, t) = -\frac{\partial u(x, 0, t)}{\partial y}, \quad \Omega(x, h, t) = -\frac{\partial u(x, h, t)}{\partial y}
\end{aligned} \tag{11(a)}$$

$$\begin{aligned}
&T(x, y, 0) = T_1, \quad T(x, 0, t) = T_1, \quad T(x, h, t) = T_2\\
&T(0, y, t) = T_1, \quad \frac{\partial T(B, y, t)}{\partial x} = 0
\end{aligned} \tag{12}$$

Equation (12) is considered unchanged for the second case while equations (10) and (11) change to the following:

$$\begin{aligned}
&\Psi(0, y, t) = 0, \quad \frac{\partial \Psi(B, y, t)}{\partial x} = 0\\
&\Psi(x, 0, t) = 0, \quad \Psi(x, h_o, t) = 0\\
&\Psi(x, y, 0) = 0\\
&u(0, y, t) = 0, \quad u(x, 0, t) = 0, \quad u(x, h_o, t) = v_o \sin(\gamma\omega t)\\
&v(0, y, t) = 0, \quad v(x, 0, t) = 0, \quad v(x, h_o, t) = 0
\end{aligned} \tag{10(b)}$$

$$\begin{aligned}
&\Omega(0, y, t) = -\varepsilon^2\frac{\partial^2 \Psi(0, y, t)}{\partial x^2}, \quad \frac{\partial \Omega(B, y, t)}{\partial x} = 0\\
&\Omega(x, 0, t) = -\frac{\partial u(x, 0, t)}{\partial y}, \quad \Omega(x, h_o, t) = -\frac{\partial u(x, h_o, t)}{\partial y}
\end{aligned} \tag{11(b)}$$

2.3 Dimensionless governing equations

The following dimensionless variables are suggested

$$X = \frac{x}{B}, \quad Y = \frac{y}{h_o} \tag{13(a, b)}$$

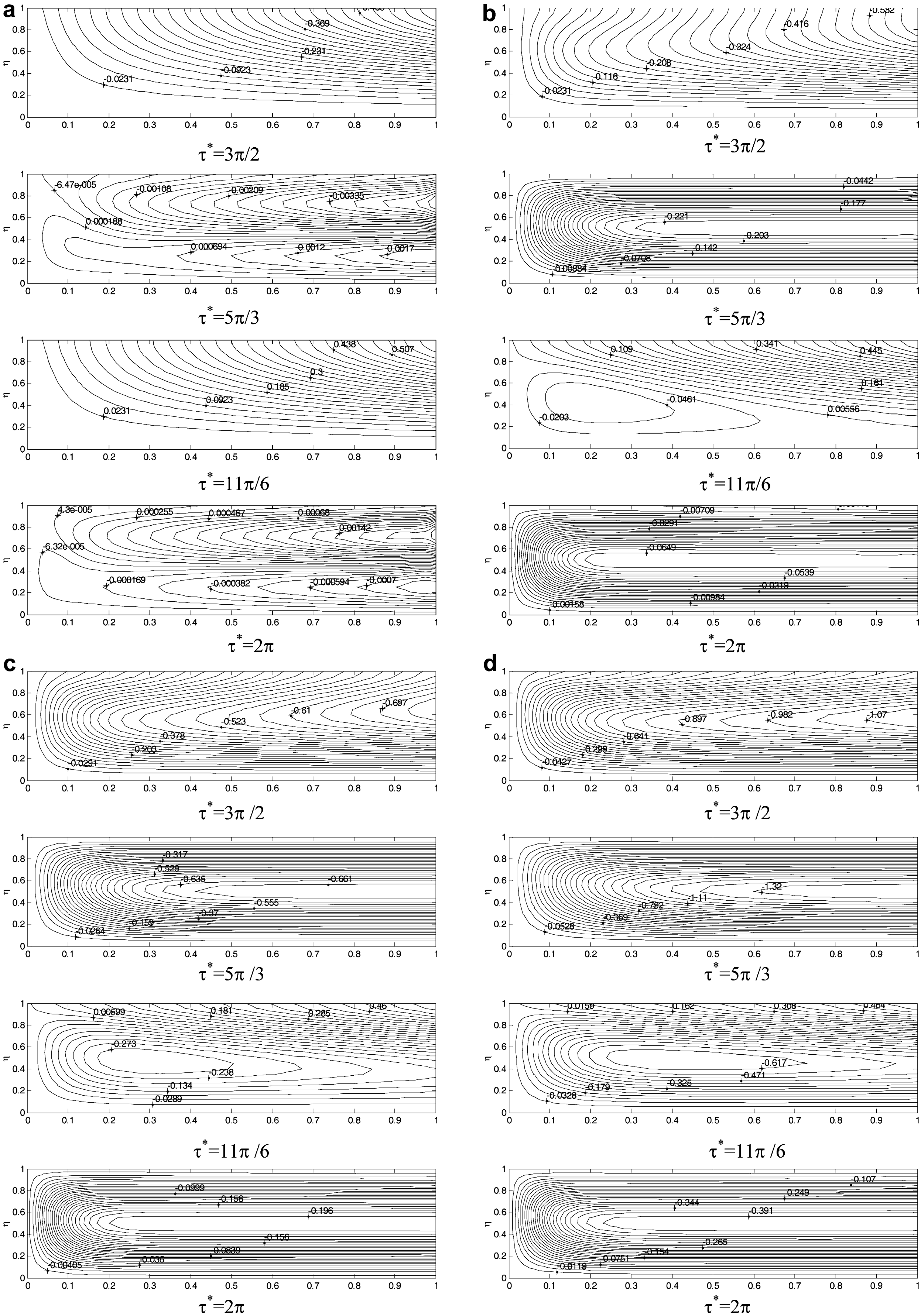
a
τ*=3π/2
τ*=5π/3
τ*=11π/6
τ*=2π
b
τ*=3π/2
τ*=5π/3
τ*=11π/6
τ*=2π
c
τ*=3π /2
τ*=5π /3
τ*=11π /6
τ*=2π
d
τ*=3π /2
τ*=5π /3
τ*=11π /6
τ*=2π

◄

Fig. 3. Dimensionless Stream Lines (Case where the Left Wall has Horizontal Motion): (a) $\frac{Gr}{R_s}=0.0$, (b) $\frac{Gr}{R_s}=200$, (c) $\frac{Gr}{R_s}=600$ and (d) $\frac{Gr}{R_s}=1200$ (Pr=1.0, R_S=1.0, ε=0.25, β=0.2, γ=3.0)

$$\tau = \omega t \tag{13(c)}$$

$$\Omega^* = \frac{\Omega}{\omega B/h_o}, \quad \Psi^* = \frac{\Psi}{h_o \omega B} \tag{13(d,e)}$$

$$\theta = \frac{T - T_1}{T_2 - T_1} \tag{13(f)}$$

where Ω^* and Ψ^* are the corresponding dimensionless values of Ω and Ψ, respectively.

Utilizing dimensionless variables listed in Equations 13(a) to 13(f) in Equation (6) results in

$$\frac{\partial \Omega^*}{\partial \tau} + \frac{\partial \Psi^*}{\partial Y}\frac{\partial \Omega^*}{\partial X} - \frac{\partial \Psi^*}{\partial X}\frac{\partial \Omega^*}{\partial Y} = \frac{1}{R_S}\left(\varepsilon^2 \frac{\partial^2 \Omega^*}{\partial X^2} + \frac{\partial^2 \Omega^*}{\partial Y^2}\right) - \frac{Gr}{R_S^2}\varepsilon \frac{\partial \theta}{\partial Y} \tag{14}$$

where Gr and ε are the Grashof number and the perturbations number, respectively which are defined as follows:

$$Gr = \frac{g\beta_o (T_2 - T_1) h_o^3}{\upsilon^2} \quad \varepsilon = \frac{h_o}{B} \tag{15}$$

The dimensionless stream function formulation and the dimensionless energy equation are:

$$\left(\varepsilon^2 \frac{\partial^2 \Psi^*}{\partial X^2} + \frac{\partial^2 \Psi^*}{\partial Y^2}\right) = -\Omega^* \tag{16}$$

$$\left(\frac{\partial \theta}{\partial \tau} + \frac{\partial \Psi^*}{\partial Y}\frac{\partial \theta}{\partial X} - \frac{\partial \Psi^*}{\partial X}\frac{\partial \theta}{\partial Y}\right) = \frac{1}{R_S Pr}\left(\varepsilon^2 \frac{\partial^2 \theta}{\partial X^2} + \frac{\partial^2 \theta}{\partial Y^2}\right) \tag{17}$$

where R_S and Pr are the modified Reynolds number and the Prandtl number of the fluid and R_S is defined as follows:

$$R_S = \frac{h_o^2 \omega}{\upsilon} \tag{18}$$

R_S is named the squeezing Reynolds number when the first case is considered because as it increases, squeezing velocities increase when the fluid and the dimensions of the channel remain unchanged. However, this number reflects the ratio of inertia forces caused by the vibrations at the left wall to induced viscous forces inside the channel for the second studied case. Therefore, it can be named as the vibrational Reynolds number.

The dimensionless boundary conditions for the first case are:

$$\begin{aligned}
&\Psi^*(0, Y, \tau) = 0, \quad \frac{\partial^2 \Psi^*(1, Y, \tau)}{\partial X^2} = 0 \\
&\Psi^*(X, 0, \tau) = 0, \quad \Psi^*(X, H, \tau) = -X\beta\gamma \sin(\gamma\tau) \\
&U(0, Y, \tau) = 0, \quad U(X, 0, \tau) = 0, \quad U(X, H, \tau) = 0 \\
&V(0, Y, \tau) = 0, \quad V(X, 0, \tau) = 0, \quad V(X, H, \tau) = \gamma\beta \sin(\gamma\tau)
\end{aligned} \tag{19(a)}$$

$$\begin{aligned}
&\Omega^*(0, Y, \tau) = -\varepsilon^2 \frac{\partial^2 \Psi^*(0, Y, \tau)}{\partial X^2}, \quad \frac{\partial^2 \Omega^*(1, Y, \tau)}{\partial X^2} = 0 \\
&\Omega^*(X, 0, \tau) = -\frac{\partial U(X, 0, \tau)}{\partial Y}, \quad \Omega^*(X, H, \tau) = -\frac{\partial U(X, H, \tau)}{\partial Y}
\end{aligned} \tag{20(a)}$$

$$\begin{aligned}
&\theta(X, 0, \tau) = 0, \quad \theta(X, H, \tau) = 1 \\
&\theta(0, Y, \tau) = 0, \quad \frac{\partial \theta(1, Y, \tau)}{\partial X} = 0 \\
&\theta(X, Y, 0) = 0
\end{aligned} \tag{21(a)}$$

where $H = \frac{h}{h_o}$. Equations 19(a) and 20(a) are changed to the following for the second case, vertical vibrations:

$$\begin{aligned}
&\Psi^*(0, Y, \tau) = 0, \quad \frac{\partial \Psi^*(1, Y, \tau)}{\partial X} = 0 \\
&\Psi^*(X, 0, \tau) = 0, \quad \Psi^*(X, 1, \tau) = 0 \\
&U(0, Y, \tau) = 0, \quad U(X, 0, \tau) = 0, \quad U(X, 1, \tau) = \frac{v_o}{\omega B} \sin(\gamma\tau) \\
&V(0, Y, \tau) = 0, \quad V(X, 0, \tau) = 0, \quad V(X, 1, \tau) = 0
\end{aligned} \tag{19(b)}$$

$$\begin{aligned}
&\Omega^*(0, Y, \tau) = -\varepsilon^2 \frac{\partial^2 \Psi^*(0, Y, \tau)}{\partial X^2}, \quad \frac{\partial \Omega^*(1, Y, \tau)}{\partial X} = 0 \\
&\Omega^*(X, 0, \tau) = -\frac{\partial U(X, 0, \tau)}{\partial Y}, \quad \Omega^*(X, 1, \tau) = -\frac{\partial U(X, 1, \tau)}{\partial Y}
\end{aligned} \tag{20(b)}$$

2.4 Thermal parameters

The thermal parameters that will be discussed are the average of the following parameters:

$$\begin{aligned}
&Nu_L(X, \tau) \equiv \frac{h_{cL} h_o}{k} = \frac{1}{1 - \theta_{AVG}(X, \tau)} \frac{\partial \theta(X, H, \tau)}{\partial Y} \\
&Nu_R(X, \tau) \equiv \frac{h_{cR} h_o}{k} = \frac{1}{\theta_{AVG}(X, \tau)} \frac{\partial \theta(X, 0, \tau)}{\partial Y}
\end{aligned} \tag{22}$$

where h_{cL} and h_{cR} are the local convective coecient at the left and right walls, respectively. Nu_L and Nu_R are the local Nusselt number at the left and right walls, respectively. θ_{AVG} is defined as follows:

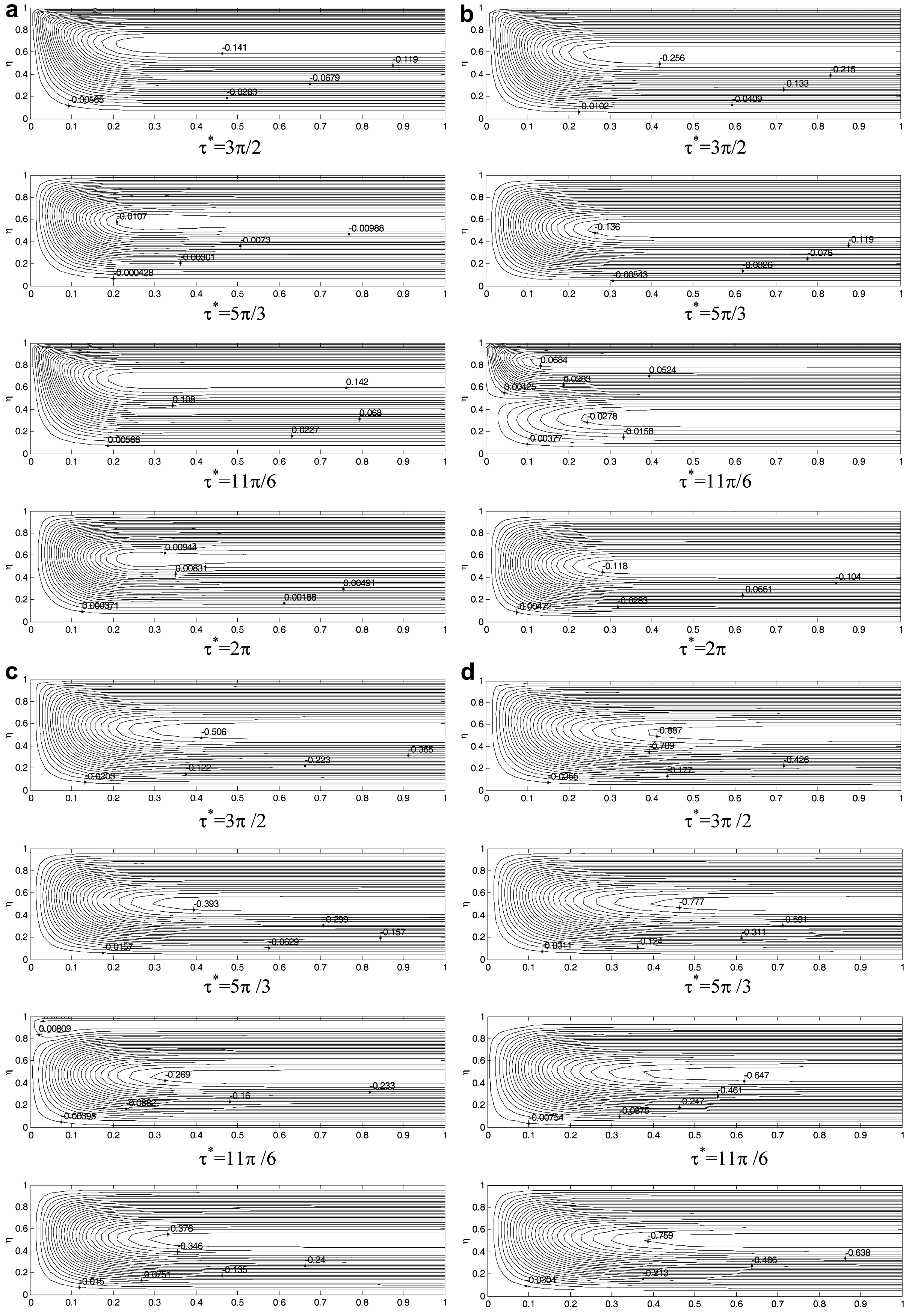
a
-0.141
-0.119
-0.0679
-0.0283
0.00565
τ*=3π/2
-0.0107
-0.00988
-0.0073
-0.00301
-0.000428
τ*=5π/3
0.142
0.108
0.068
0.0227
0.00566
τ*=11π/6
0.00944
0.00831
0.00491
0.00188
0.000371
τ*=2π
b
-0.256
-0.215
-0.133
-0.0409
-0.0102
τ*=3π/2
-0.136
-0.119
-0.076
-0.0326
-0.00543
τ*=5π/3
0.0684
0.0524
0.0283
0.00425
-0.0278
-0.0158
-0.00377
τ*=11π/6
-0.118
-0.104
-0.0661
-0.0283
-0.00472
τ*=2π
c
-0.506
-0.365
-0.223
-0.122
-0.0203
τ*=3π /2
-0.393
-0.299
-0.157
-0.0629
-0.0157
τ*=5π /3
0.00809
-0.269
-0.233
-0.16
-0.0882
-0.00395
τ*=11π /6
-0.376
-0.346
-0.24
-0.135
-0.0751
-0.015
τ*=2π
d
-0.887
-0.709
-0.426
-0.177
-0.0355
τ*=3π /2
-0.777
-0.591
-0.311
-0.124
-0.0311
τ*=5π /3
-0.647
-0.461
-0.247
-0.0875
-0.00754
τ*=11π /6
-0.769
-0.638
-0.486
-0.213
-0.0304
τ*=2π

◄

Fig. 4. Dimensionless Stream Lines (Case where the Left Wall has Vertical Motion): (a) $\frac{Gr}{R_S} = 0.0$, (b) $\frac{Gr}{R_S} = 200$, (c) $\frac{Gr}{R_S} = 600$ and (d) $\frac{Gr}{R_S} = 1200$ (Pr=1.0, R_S=1.0, ε=0.25, $\frac{v_o}{\omega B} = 1.0$, γ=3.0)

$$\theta_{AVG}(X,\tau) = \frac{1}{H}\int_0^H \theta(X,Y,\tau)\,dY \tag{23}$$

2.5 Analytical solution

Equations (14) and (17) can be reduced to the following for small values of the following parameters: R_S, Pr and ε numbers

$$\frac{\partial^2\Omega^*}{\partial Y^2} = \frac{Gr}{R_S}\varepsilon\frac{\partial\theta}{\partial Y} \tag{24}$$

$$\frac{\partial^2\theta}{\partial Y^2} = 0 \tag{25}$$

Accordingly, the dimensionless analytical solutions for the velocities, temperature and thermal parameters are listed below for the first case:

$$U(X,Y,\tau) \equiv \frac{u}{\omega B} = -\frac{Gr}{R_S}\varepsilon H^2\left[\frac{1}{6}\left(\frac{Y}{H}\right)^3 - \frac{1}{4}\left(\frac{Y}{H}\right)^2 + \frac{1}{12}\left(\frac{Y}{H}\right)\right] + \frac{6X\beta\gamma\sin(\gamma\tau)}{H}\left[\left(\frac{Y}{H}\right)^2 - \left(\frac{Y}{H}\right)\right] \tag{26(a)}$$

$$V(X,Y,\tau) \equiv \frac{v}{h_o\omega} = \beta\gamma\sin(\gamma\tau)\left[3\left(\frac{Y}{H}\right)^2 - 2\left(\frac{Y}{H}\right)^3\right] \tag{27(a)}$$

$$\theta(X,Y,\tau) = \left(\frac{Y}{H}\right) \tag{28(a)}$$

$$Nu_L = Nu_R = \frac{2.0}{H} \tag{29(a)}$$

The corresponding solutions for the second case are

$$U(X,Y,\tau) \equiv \frac{u}{\omega B} = -\frac{Gr}{R_S}\varepsilon\left[\frac{Y^3}{6} - \frac{Y^2}{4} + \frac{Y}{12}\right] + \frac{v_o}{\omega B}\sin(\gamma\tau)\left[3Y^2 - 2Y\right] \tag{26(b)}$$

$$V(X,Y,\tau) = 0 \tag{27(b)}$$

$$\theta(X,Y,\tau) = Y \tag{28(b)}$$

$$Nu_L = Nu_R = 2.0 \tag{29(b)}$$

3 Numerical analysis

Equations (14), (16) and (17) were transformed from X, Y and τ domain into a new computational domain, ξ=X, $\eta = \frac{Y}{H}$ and $\tau^* = \tau$. The transformed equations are

$$H^2\frac{\partial\Omega^*}{\partial\tau^*} + UH^2\frac{\partial\Omega^*}{\partial\xi} + \left[V - \eta\frac{dH}{d\tau^*}\right]H\frac{\partial\Omega^*}{\partial\eta} = \frac{1}{R_S}\left(\varepsilon^2H^2\frac{\partial^2\Omega^*}{\partial\xi^2} + \frac{\partial^2\Omega^*}{\partial\eta^2}\right) - \frac{Gr}{R_S^2}\varepsilon H\frac{\partial\theta}{\partial\eta} \tag{30}$$

$$\left(\varepsilon^2H^2\frac{\partial^2\Psi^*}{\partial\xi^2} + \frac{\partial^2\Psi^*}{\partial\eta^2}\right) = -\Omega^*H^2 \tag{31}$$

$$\left(H^2\frac{\partial\theta}{\partial\tau^*} + UH^2\frac{\partial\theta}{\partial\xi} + \left[V - \eta\frac{dH}{d\tau^*}\right]H\frac{\partial\theta}{\partial\eta}\right) = \frac{1}{R_S\,Pr}\left(\varepsilon^2H^2\frac{\partial^2\theta}{\partial\xi^2} + \frac{\partial^2\theta}{\partial\eta^2}\right) \tag{32}$$

where H and $\frac{dH}{d\tau^*}$ are equal to unity and zero for the second case, respectively. Equations (30) and (32) were solved using an alternating direction implicit ADI method. The procedure is based on dividing each time step in two halves where equations (30) and (32) are swept in the ξ and η directions in the first and second halves of each time step, respectively, as discussed by Hoffmann and Chiang [17]. Center differencing in space was used for discretizing the dimensionless vorticity and temperature differential terms and forward differencing was used to approximate time differential terms. These discretizations resulted in tridiagonal systems for each half time step which can be solved efficiently using Thomas Algorithm (Blottner [18]). After each half time step, equation (31) was solved using the method of successive over relaxation SOR.

The dimensionless velocities in equation (30), dimensionless vorticity at the walls and the dimensionless temperature were calculated at previous half time steps. Then, the vorticity equation was solved for the vorticity field. Accordingly, the stream function formulation was solved and an approximate velocity field was obtained for the current time. Next, the dimensionless temperature was obtained from equation (32). The obtained velocities along with the calculated temperatures were used again in the vorticity equation at the current time to correct for the dimensionless velocities, boundary conditions and temperature gradients for equation (30). The preceding steps are repeated until the velocity field did not change with iterations for the current time. Accordingly, the temperature, stream function and the vorticity fields were obtained for the current time step. Finally, the previous procedure were repeated for the next consecutive time steps. Similar procedures that can be applied for the ADI solution are found in the literature (Example: El-Refaee et. al. [19]).

The value of γ in equation (1) was chosen to be 3 to reduce number of time steps. Note that other values of γ will result in similar physical behavior. Based on extensive numerical experimentation, the values of 0.0125, 0.05, 0.001, 10^{-6} and 10^{-6} were chosen for $\Delta\xi$, $\Delta\eta$, $\Delta\tau^*$, maximum error for stream functions in equation (31) and the maximum error in the velocity field, respectively. These values resulted in grid and time independent solutions.

The numerical results of equations (30) through (32) for the dimensionless axial velocities were compared with the corresponding analytical solutions derived in this work. The results of the comparisons were found to be in excellent agreement as shown in Figs. 2(a, b) for both studied cases. Accordingly, the above equations were solved for various values of squeezing/vibrational Reynolds number and Grashof number in order to better understand the behavior of natural convection inside a vibrated vertical channel.

4
Discussion of the results

Figure 3 shows the effects of the Gr on the stream lines for the cases where the left wall is vibrating horizontally. It is noted that a cell originates at the lower right portion of the vertical channel at relatively low values of Grashof number during squeezing stages, $\frac{5\pi}{3} \le \tau^* \le 2\pi$. As the Gr increases, suction velocities near the right wall increase such that they can exceed the induced squeezed velocities due to vibration. As a result, this cell collapses and the flow achieves normal conditions for large Gr values. This could create a problem in controlling the outdoor vibrations since they can affect the ventilation rate in thermal comfort applications. Also, this phenomenon can create problem in open chambers that are used for measuring the concentration of specific species since this cell can isolate the measuring device resulting in inaccurate measurements.

Figure 4 shows the effects of the Grashof number on the stream lines for the case where the left wall is vibrating vertically. The interesting feature of this type of motion can be seen in the time period $\frac{5\pi}{3} \le \tau^* \le 2\pi$, especially at $\tau^* = \frac{11\pi}{6}$, where the left wall speed is negative. It is noticed that two separate flow zones are created at low Grashof numbers during this time period. Flow enters the channel from both the left and the right wall regions. These flows exit in turn from the central portion of the channel. As Gr increases, buoyancy induced flow velocities increase over the induced vibrational flow thus normal flow trends are recovered as shown in Fig. 4(d).

Figure 5 illustrates the effects of R_S on isotherms for the first case. It is noticed that as R_S increases, axial convection increases resulting in a maximum convections during squeezing stages for the first case. Note that R_S can be increased by increasing the vibrational frequency. Fig. 6 represents the effects of both R_S and $v_o/\omega B$ on

Fig. 5. Dimensionless Isotherms (Case where the Left Wall has Horizontal Motion): (a) $R_S = 1.0$, (b) $R_S = 10$ ($Pr = 1.0$, $\frac{Gr}{R_S} = 600$, $\varepsilon = 0.25$, $\beta = 0.2$, $\gamma = 3.0$)

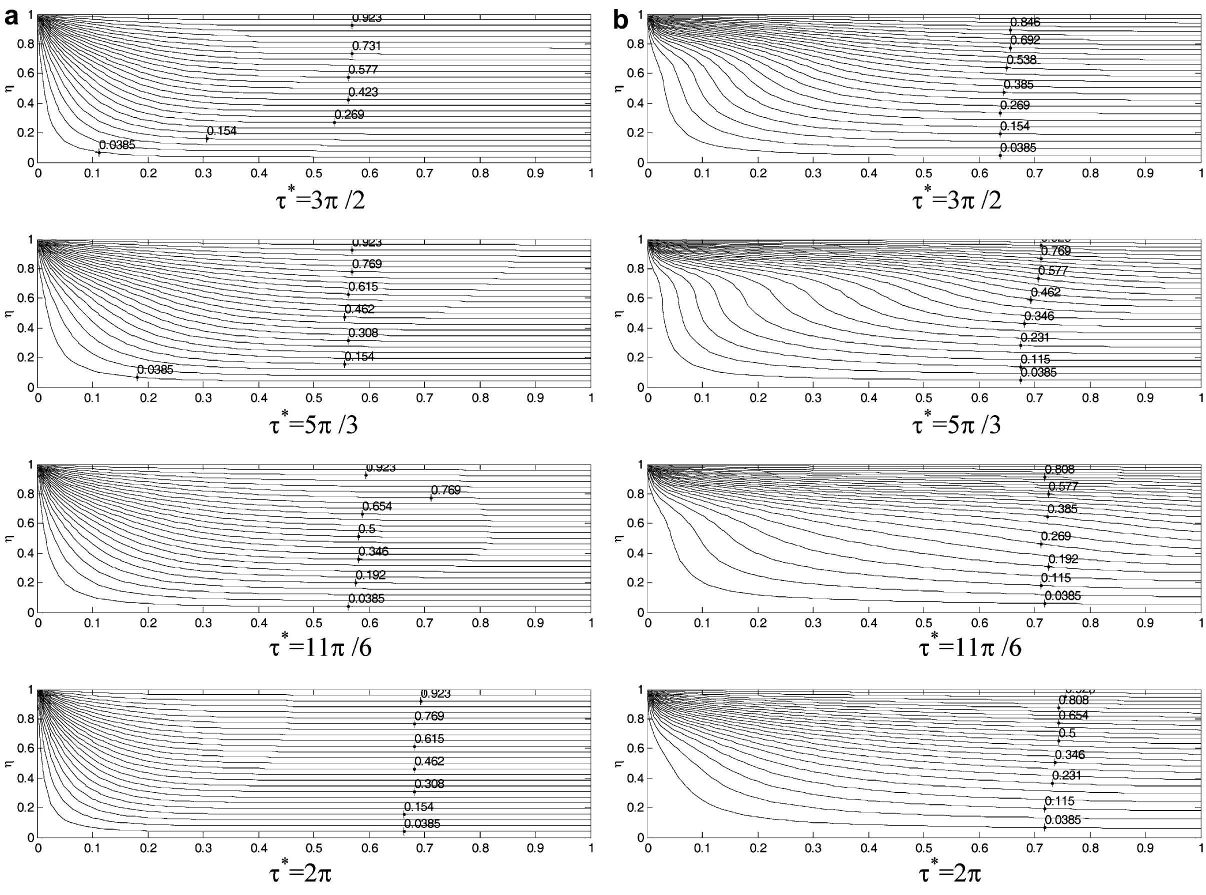

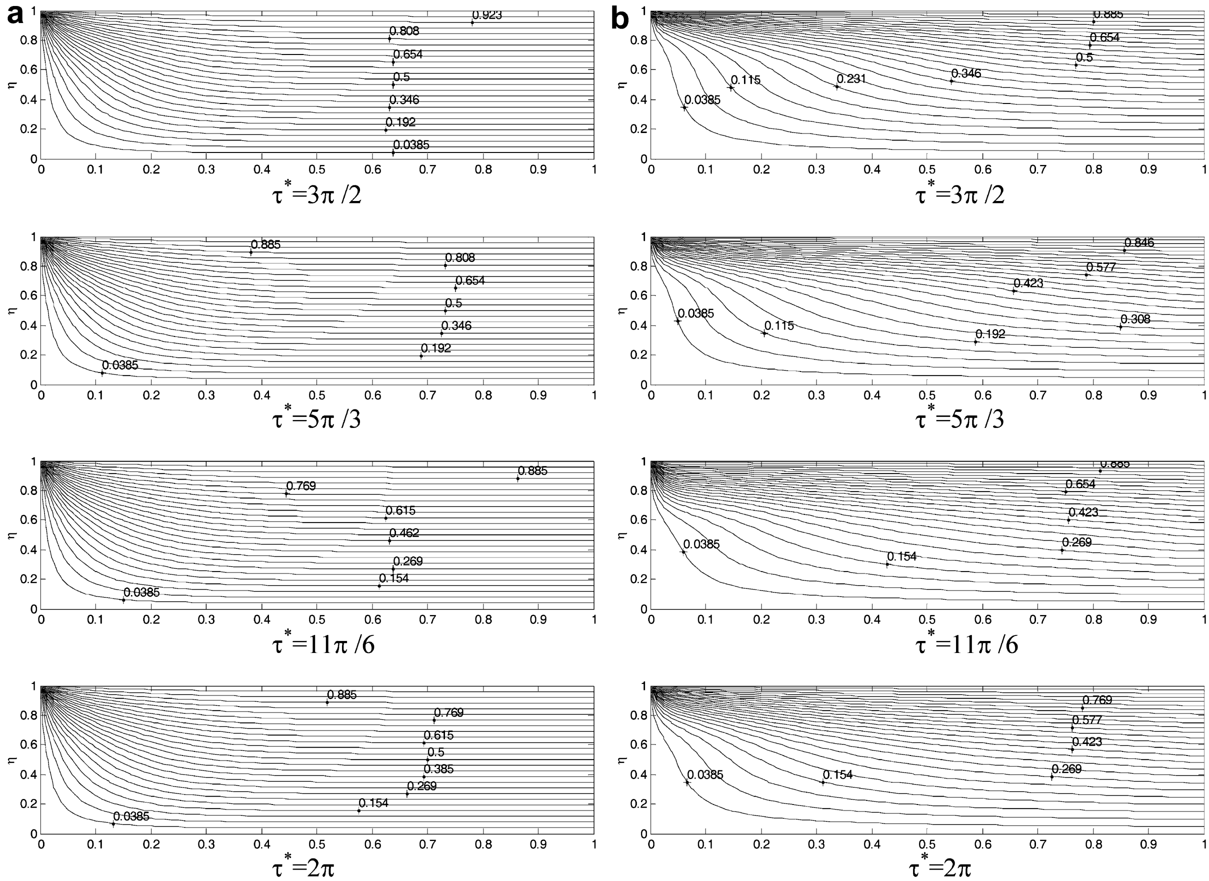

Fig. 6. Dimensionless Isotherms (Case where the Left Wall has Vertical Motion): (a) $R_S = 1.0$, (b) $R_S = 10$ (Pr=1.0, $Gr/R_S = 600$, $\varepsilon = 0.25$, $v_o/\omega B = 1.0$, $\gamma = 3.0$)

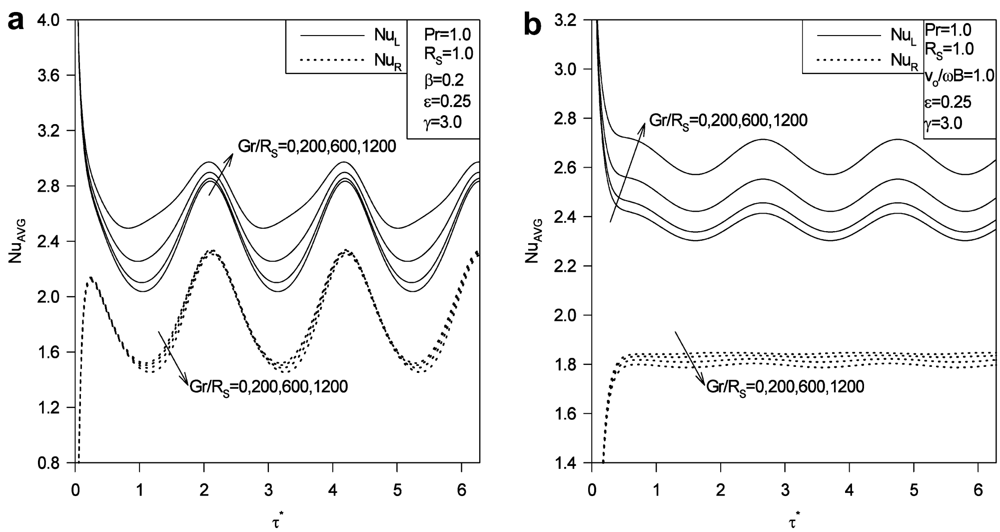

Fig. 7. Effects of $\frac{Gr}{R_S}$ on Nusselt numbers ($R_S = 1.0$): Left wall having oscillatory (a) horizontal and (b) vertical motion

isotherms for the second case. As both R_S and v_o increase, axial convections increase, reaching their maximum values when the wall speed reaches its maximum positive values.

Figure 7 displays the effects of the $\frac{Gr}{R_S}$ on the average Nusselt number for both cases at a low R_S value. It is noticed that the fluctuations in Nusselt numbers are greater when the left wall oscillates horizontally as compared to when it oscillates vertically. Equations 26(a) and 26(b) suggest that horizontal vibrations affect both buoyancy forces and the flow induced by the motion of the wall yet vertical vibrations affect mainly the flow induced by vibrations. The interaction in the first case between vibrations and the oscillatory buoyancy forces resulted from

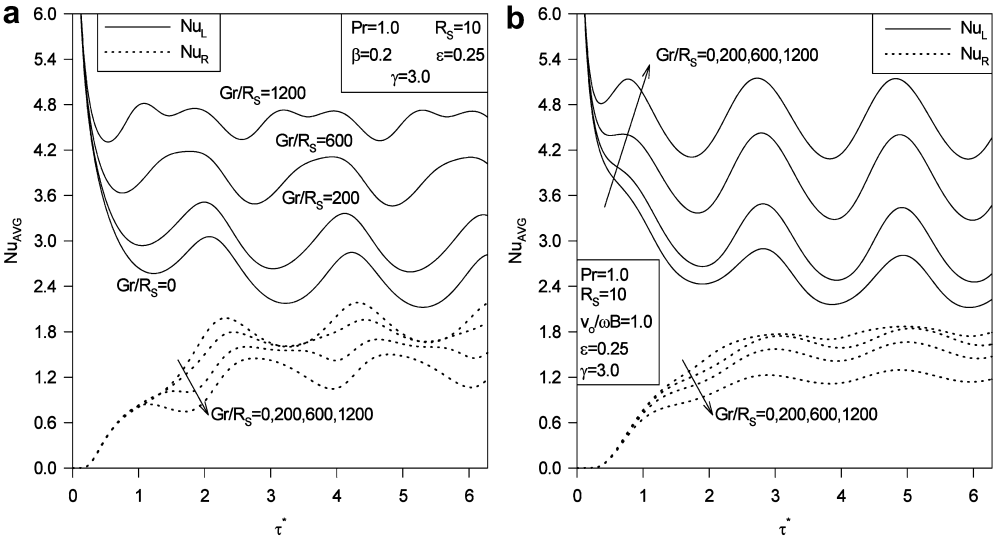

Fig. 8. Effects of $\frac{Gr}{R_S}$ on Nusselt numbers ($R_S = 10$): Left wall having oscillatory (a) horizontal and (b) vertical motion

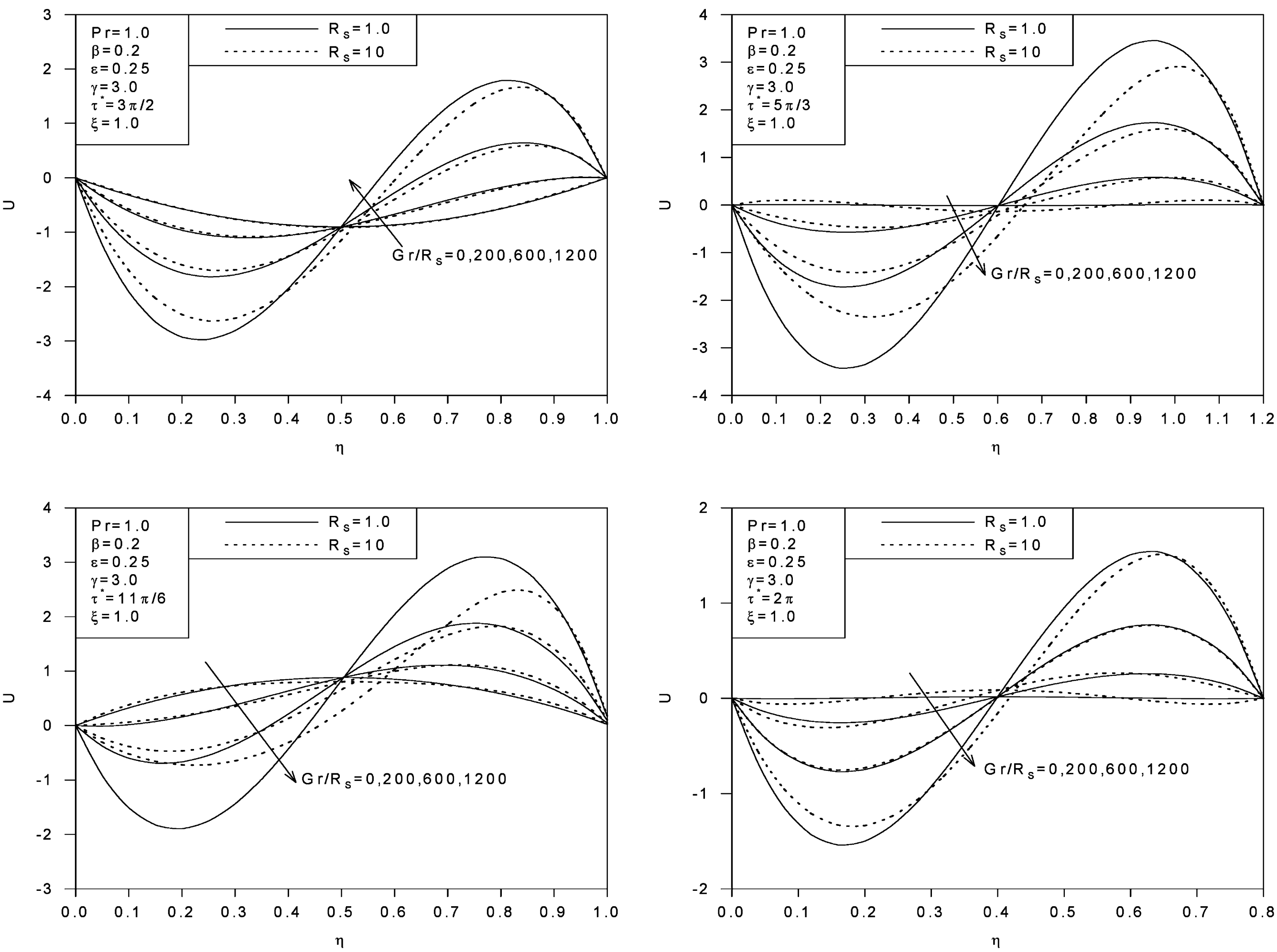

Fig. 9. Effects of $\frac{Gr}{R_S}$ on U (Case where the Left Wall has Horizontal Motion)

variations in the channel thickness cause the trend of the average Nusselt number to change as $\frac{Gr}{R_S}$ increases.

Amplitude of oscillations for Nusselt numbers decrease as $\frac{Gr}{R_S}$ increases at the vibrated wall for horizontal vibrations because a substantial increase in the Nusselt number at maximum thickness is expected due to buoyancy effects. However, these amplitudes are less affected by $\frac{Gr}{R_S}$ for the second case. Fluid temperatures inside the channel are expected to decrease as the Grashof number increases due to enhancements in thermal convections. Therefore, average Nusselt numbers at the vibrated wall increase as $\frac{Gr}{R_S}$ increases while it is decreased at the fixed wall with

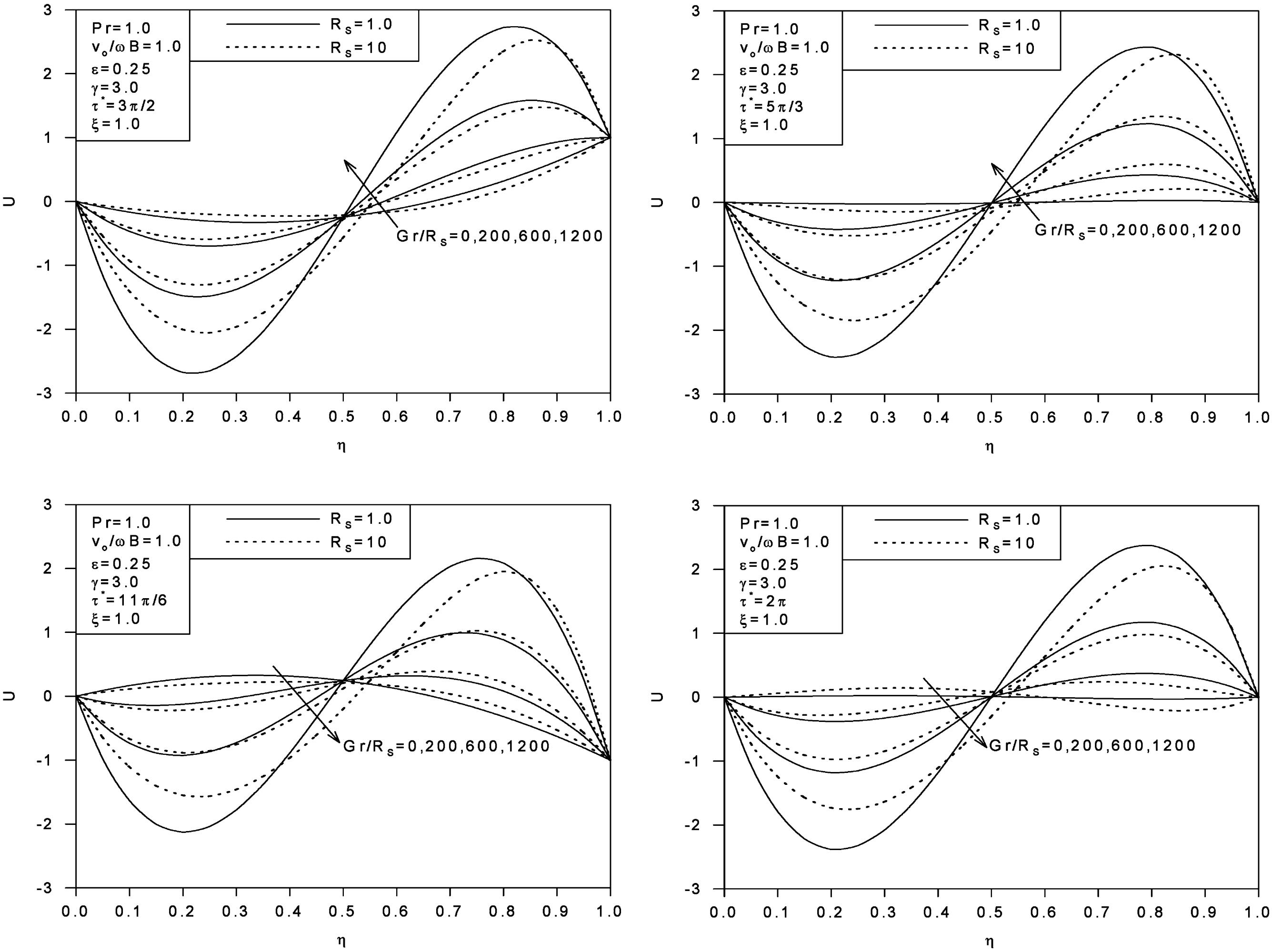

Fig. 10. Effects of $\frac{Gr}{R_S}$ on U (Case where the Left Wall has Vertical Motion)

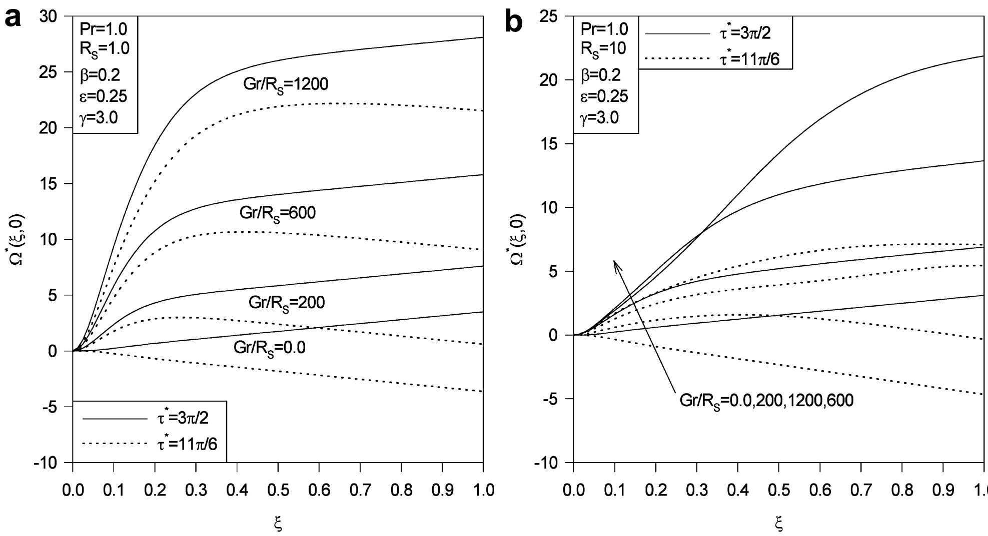

Fig. 11. Effects of $\frac{Gr}{R_S}$ on $\Omega^*(\xi, 0)$ (Case where the Left Wall has Horizontal Motion)

increases in $\frac{Gr}{R_S}$. The suggested correlations that are presented in the next subsection show that mean Nusselt numbers are less affected by R_S at fixed values of Gr.

Dimensionless axial velocity profiles for horizontal and vertical vibrational modes are seen in Figs. 9 and 10, respectively. It can be seen that induced velocities increase as $\frac{Gr}{R_S}$ increases. Also, it is noticed that as R_S increases, the flow becomes more attached to the left wall, the source of disturbance. The effects of $\frac{Gr}{R_S}$ on dimensionless vorticity at the right wall $\Omega^*(\xi, 0)$ are shown in Figs. 11 and 12 for two different R_S values. As $\frac{Gr}{R_S}$ increases, $\Omega^*(\xi, 0)$ increases for both horizontal and vertical vibrational modes. Further, it should be noted that as R_S increases, instabilities in $\Omega^*(\xi, 0)$ start to appear at larger values of $\frac{Gr}{R_S}$ as shown in Fig. 12(b).

4.1 Correlations

Tables (1) and (2) contain correlations for the mean value of the average Nusselt numbers, $(Nu_{L,Ravg})_{mean}$, at the right and left walls and their corresponding fluctuation, $\Delta Nu_{L,Ravg}$. These are defined as follows:

$$(Nu_{L,Ravg})_{mean} \cong \frac{\gamma}{2\pi} \int_{2\pi\left(1-\frac{1}{\gamma}\right)}^{2\pi} Nu_{L,Ravg}(\tau^*)\, d\tau^* \tag{33}$$

$$\Delta Nu_{L,Ravg} = \frac{(Nu_{L,Ravg})_{Max} - (Nu_{L,Ravg})_{Min}}{2} \tag{34}$$

where $(Nu_{L,Ravg})_{Max}$ and $(Nu_{L,Ravg})_{Min}$ are the maximum and minimum average Nusselt numbers. In these correlations, $Nu_{L,Ravg}$ stands for either Nu_{Lavg} or Nu_{Ravg} which are the average Nusselt numbers for the left or the right walls, respectively. The listed correlations are derived for a

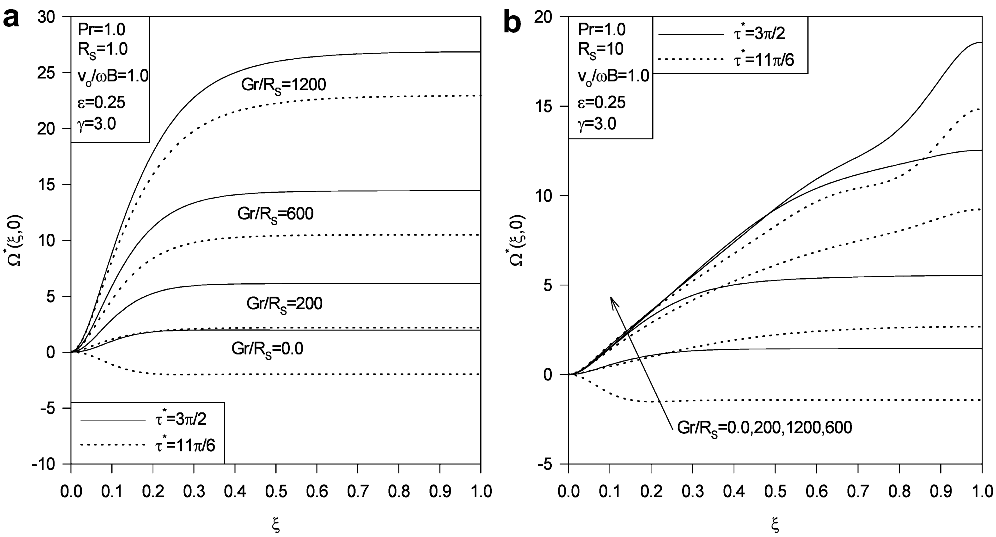

Fig. 12. Effects of $\frac{Gr}{R_S}$ on $\Omega^*(\xi, 0)$ (Case where the Left Wall has Horizontal Motion)

Table 1. Correlations for Nusselt numbers and their corresponding fluctuations for left wall expressing a horizontal vibration (Pr=1.0, ε = 0.25 and γ = 3.0, 0 $\leq$ R_S $\leq$ 5, 0 $\leq$ Gr/R_S $\leq$ 1000, 0 $\leq$ β $\leq$ 0.3

Correlations for horizontal vibration	Maximum error
$(Nu_{Lavg})_{mean} = \frac{2.298(1+R_S)^{0.0134}}{(1-\beta^2)^{0.4599}} + 4.725(10^{-4})(50 + Gr)^{0.9214}$	1%
$\frac{\Delta Nu_{Lavg}}{(Nu_{Lavg})_{mean}} = \frac{2.147\beta^{1.067}}{(110+Gr)^{0.1733}(1+R_S)^{0.01734}}$	14%
$(Nu_{Ravg})_{mean} = \frac{2.682}{(110+Gr)^{0.02355}} - 0.4564(1 + R_S)^{0.1548}(1 - \beta^2)^{2.237}$	5%
$\frac{\Delta Nu_{Ravg}}{(Nu_{Ravg})_{mean}} = 0.9326\beta^{1.042}(110 + Gr)^{0.04196}$	1%, $R_S = 1$

Table 2. Correlations for Nusselt numbers and their corresponding fluctuations for left wall expressing a vertical vibration (Pr = 1.0, ε = 0.25 and γ = 3.0, 0 $\leq$ R_S $\leq$ 5, 0 $\leq$ Gr/R_S $\leq$ 1000, 0.5 $\leq$ $v_o/\omega B$ $\leq$ 2.0)

Correlations for vertical vibration	Maximum error
$(Nu_{Lavg})_{mean} = 2.3093(1 + R_S)^{0.0118}\left(1 + \frac{v_o}{\omega B}R_S\right)^{0.0106} + 2.5979(10^{-4})Gr^{0.96623}$	1%
$\frac{\Delta Nu_{Lavg}}{(Nu_{Lavg})_{mean}} = \frac{0.02442\left(\frac{v_o}{\omega B}R_S\right)^{0.9365}}{(1+R_S)^{0.3096}}\left(110 + \frac{Gr}{R_S}\right)^{0.0417}$	9%
$(Nu_{Ravg})_{mean} = \frac{1.9535\left(1+\frac{v_o}{\omega B}R_S\right)^{0.005634}}{(1+R_S)^{0.0447}} - 1.9933(10^{-4})\left(\frac{Gr}{R_S}\right)^{0.9296}$	4%
$\frac{\Delta Nu_{Ravg}}{(Nu_{Ravg})_{mean}} \cong 0$	

Prandtl number equal to unity and a perturbation parameter equal to one-fourth. The maximum value of R_S was selected to be 5. As such these correlations are valid for actual vibrational frequency less than 2 s^{-1} for a vertical channel having a thickness equal to 10–20 mm.

In addition to the above correlations, the steady periodic behavior for the average Nusselt number at either left or right wall, for the horizontal vibrational case, can be approximated by the following correlation for relatively low values of $\frac{Gr}{R_s}$ ratio:

$$\mathrm{Nu}_{L,Ravg}(t) = \frac{(\mathrm{Nu}_{L,Ravg})_{mean}\sqrt{1-\beta^2}}{1-\beta\cos(\gamma\omega t)} \tag{35}$$

The developed correlations show that the amplitude of Nusselt numbers at the vibrated wall decreases especially for vertical vibrations as squeezing/vibrational Reynolds number increases at constant Gr. Also, they show that amplitudes of Nusselt numbers are increased by increases in amplitudes of the vibration for both studied modes.

5
Conclusions

Heat transfer and flow induced by both natural convection and vibrations within an open-end vertical channel have been analyzed in this work. The left wall of the vertical channel was allowed to have either horizontal or vertical vibrations. The reduced dimensionless vorticity-stream function formulations and the energy equation have been solved numerically. Their results for a special case were compared with an analytical solution which was derived in this work under similar conditions. Excellent agreement was found between analytical and numerical results. Oscillatory horizontal vibrations at the left wall result in a separated cell inside the vertical channel at low Grashof numbers. Mean values for average Nusselt numbers at the vibrated wall were found to be mainly affected by the Grashof number and the amplitude of horizontal vibrations. The amplitude of Nusselt numbers was found to increase with increases in the amplitude of vibrations for vertical and horizontal modes of vibrations. However, it decreases at the vibrated wall with an increase in the Grashof number for horizontal vibrations. Average Nusselt numbers at non-vibrated wall decrease with an increase the Grashof number. It was also found that disturbances in the Nusselt numbers are more prominent the horizontal oscillations as compared to the vertical oscillations.

References

1. Daloglu A; Ayhan T (1999) Natural Convection in a Periodically Finned Vertical Channel. International Communication Heat Mass Transfer 26: 1175–1182
2. Writz RA; Stutzman RJ (1982) Experiments on Free Convection between Vertical Plates with Symmetric Heating. Journal of Heat Transfer 104: 501–507
3. Ramanathan S; Kumar R (1991) Correlations for Natural Convection between Heated Vertical Plates. Journal of Heat Transfer 113: 97–107
4. Vafai K; Ettefagh J (1990a) The Effects of Sharp Corners on Buoyancy-Driven Flows with Particular Emphasis on Outer Boundaries. International Journal of Heat and Mass Transfer 33: 2311–2328
5. Vafai K; Ettefagh J (1990b) Thermal and Fluid Flow Instabilities in Buoyancy-Driven Flows in Open-Ended Cavities. International Journal of Heat and Mass Transfer 33: 2329–2344
6. Khanafer K; Vafai K (2000) Buoyancy-driven flow and heat transfer in open-ended enclosures: elimination of the extended boundaries. International Journal of Heat and Mass Transfer 43: 4087–4100
7. Morrone B (2001) Natural Convection between Parallel Plates with Conjugate Conductive Effects. Numerical Heat Transfer, Part A-Applications 40: 873–886
8. Paul T; Singh AK; Thorpe GR (1999) Transient Natural Convection in a Vertical Channel Partially Filled with a Porous Medium. Mathematical Engineering in Industry 7: 441–455
9. Barozzi GS; Corticelli MA (2000) Natural Convection in Cavities Containing Internal Sources. Heat and Mass Transfer 36: 473–480
10. Kuan-Tzong L (1999) Laminar Natural Convection Heat and Mass Transfer in Vertical Rectangular Duct. International Journal of Heat and Mass Transfer 42: 4523–4534
11. Zamora B; Hernandez J (1997) Influence of Variable Property Effects on Natural Convection Flows in Asymmetrically-heated Vertical Channels. International Communications in Heat and Mass Transfer 24: 1153–1162
12. Bessaih R; Kadja M (2000) Turbulent natural convection cooling of electronic components mounted on a vertical channel. Applied Thermal Engineering 20: 141–154
13. Hall DA; Vliet GC; Bergman TL (1999) Natural Convection Cooling of Vertical Rectangular Channels in Air Considering Radiation and Wall Conduction. Transactions of the ASME. Journal of Electronic Packaging 121: 75–84
14. Dalal DC; Datta N; Mukherjea SK (1998) Unsteady Natural Convection of a Dusty Fluid in an Infinite Rectangular Channel. International Journal of Heat and Mass Transfer 41: 547–562
15. Fu WS; Shieh WJ (1993) Transient Thermal-Convection in an Enclosure Induced Simultaneously by Gravity and Vibration. International Journal of Heat and Mass Transfer 36: 437–452
16. Kwak HS; Kuwahara K; Hyun JM (1998) Resonant Enhancement of Natural Convection Heat Transfer in a Square Enclosure. International Journal of Heat and Mass Transfer 41: 2837–2846
17. Hoffmann KA; Chiang ST (1998) Computational Fluid Dynamics: Volume I. Third Edition. Wichita. Kansas: Engineering Education System: 337–352
18. Blottner FG (1970) Finite-Difference Methods of Solution of the Boundary-Layer Equations. AIAA Journal 8: 193–205
19. El-Refaee MM; Elsayed MM; Al-Najem NM; Noor AA (1998) Natural Convection in Partially Cooled Tilted Cavities. International Journal for Numerical Methods in Fluid 28: 477–499